Doping dependence of the electronic structure and the Raman-active modes in $La_{2-x}Ba_xCuO_4$

T. Thonhauser and C. Ambrosch-Draxl
Institut für Theoretische Physik, Universität Graz, Universitätsplatz 5, A-8010 Graz, Austria
(Received 6 February 2002; revised manuscript received 30 January 2003; published 4 April 2003)

We studied the doping dependence of the electronic structure and the Raman-active phonon modes in the high-temperature superconductor $La_{2-x}Ba_xCuO_4$. Thereby, doping concentrations from the undoped case ($x=0$) up to the overdoped case ($x=0.14$) were considered. All obtained phonon frequencies compare well to published data for $La_{2-x}Sr_xCuO_4$. For optimal doping of $x_{opt}\approx 0.12$ the A_{1g} Raman spectra show a huge increase in intensity for certain scattering geometries indicating enhanced electron-phonon coupling. The effects of doping on the density of states, Fermi surface, and electric-field gradients were also investigated.

DOI: 10.1103/PhysRevB.67.134508 PACS number(s): 74.25.Kc, 74.25.Jb, 78.30.−j, 71.15.Mb

I. INTRODUCTION

The discovery of superconductivity in doped La_2CuO_4 by Bednorz and Müller[1] marked the beginning of the high temperature superconductivity era. Upon doping with Ba or Sr, this copper oxide shows superconductivity with transition temperatures T_c of up to more than 30 K. Although many experimental and theoretical results have already been published, this material is still of great interest for the search of the pairing mechanism. It is generally believed now that the high transition temperatures in superconductors cannot be mediated by electron-phonon coupling only. Nevertheless, there are many indications that phonons play a leading role in the explanation of high-T_c superconductivity.[2,3] In addition, Raman and neutron scattering provide much information about the lattice as well as the electronic states and have therefore been studied intensively.

Many of the experiments and most of the calculations were done for the undoped or Sr-doped system $La_{2-x}Sr_xCuO_4$,[4–10] while for the Ba-doped case there are hardly any investigations for the electronic structure[11] and lattice dynamics. This may be a result of the fact that the maximal transition temperature of the Sr-doped compound is 38 K, while it is just 30 K when doped with Ba.

As in many other compounds, phonon frequencies have been studied with different experimental probes, but much less is known about the corresponding eigenvectors. It has been shown recently for the high temperature superconductor $YBa_2Cu_3O_7$ that upon isotope substitution the change in the eigenvectors can lead to dramatic effects in the Raman intensities.[12] For the superconducting rare-earth carbide halides[13] the calculated Raman spectra could contribute by assigning the experimentally measured Raman-active phonon modes. For $La_{2-x}Sr_xCuO_4$ neutron-scattering measurements showed a controversy concerning the softening of the highest LO phonon branch.[14,15] A similar phonon anomaly was found theoretically for the Ba-doped compound.[16] For all these reasons it is important to theoretically characterize the lattice dynamics of materials.

Independent of the quasiparticle mediating the pairing mechanism the electronic structure itself is an important quantity for superconductivity. Upon doping, the three-valent La is replaced by two-valent Ba/Sr which leads to the creation of holes in the CuO_2 planes. Thus a detailed knowledge of the doping dependence of the electronic structure can provide more insight into superconductivity in the cuprates.

In this paper we theoretically investigate the effect of doping on the electronic structure as well as on all Raman-active modes of $La_{2-x}Ba_xCuO_4$. Special focus is given to the charge redistribution in the copper-oxygen planes upon doping. Experimentally measurable properties such as the density of states (DOS), electric-field gradients (EFG's), and Raman spectra are calculated.

II. CRYSTAL STRUCTURE AND SYMMETRY

The crystal structure of La_2CuO_4 exhibits a phase transition from the high-temperature tetragonal phase above about 515 K to the low-temperature orthorhombic phase. The phase-transition temperature decreases with the increase of Ba or Sr content[17] and is about 300 K for $x=0.035$. Unlike $La_{2-x}Sr_xCuO_4$, $La_{2-x}Ba_xCuO_4$ with $x\approx 0.12$ undergoes a second transition to a low-temperature tetragonal phase below 60 K. We have investigated this phase considering the corresponding $I4/mmm$ symmetry for all our calculations. Henceforth, the oxygen in the CuO_2 plane will be denoted as O1 and the apical oxygen will be referred to as O2.

From structure and symmetry considerations it follows that the full phonon spectrum consists of 21 phonon modes, three acoustic and 18 optic modes. Further, one finds that the Brillouin zone-center phonons can be characterized according to $\Gamma_{vib}=2A_{1g}+3A_{2u}+B_{2u}+2E_g+4E_u$. The A_{1g} and E_g modes conserve inversion symmetry and therefore they are Raman active. The A_{1g} modes correspond to vibrations of the La and apical O along the c axis, while the E_g modes are characterized by movements of these atoms parallel to the CuO_2 planes.

The components of the Raman tensor χ for the A_g modes are given by

$$\chi(A_g)=\begin{pmatrix} a & 0 & 0 \\ 0 & a & 0 \\ 0 & 0 & b \end{pmatrix}. \qquad (2.1)$$

Therefore, two different spectra are of interest, i.e., the (xx)-polarized and the (zz)-polarization spectra. (xx) means that the incoming and outgoing light are polarized parallel to the x axis. For E_g modes the tensor takes the form

$$\chi(E_g,x)=\begin{pmatrix} 0 & 0 & -a \\ 0 & 0 & 0 \\ -a & 0 & 0 \end{pmatrix}, \quad \chi(E_g,y)=\begin{pmatrix} 0 & 0 & 0 \\ 0 & 0 & a \\ 0 & a & 0 \end{pmatrix}, \tag{2.2}$$

which means that the (xz)- and (yz)-polarized spectra are identical and all others vanish.

III. METHOD

A. Computational details

All calculations are performed within the full-potential linearized augmented plane-wave (LAPW) method as implemented in the WIEN97 code.[18] In the wave-function expansion 900 basis functions have been used. This corresponds to a $RK_{\max}$ value of 7 for the oxygen, where the muffin-tin radii have been chosen to be 2.4 (La), 1.9 (Cu), and 1.6 (O) bohr. The potentials and charge densities are represented by 1765 stars in the interstitial region, and by spherical harmonics up to $L=6$ within the muffin-tin spheres. For Brillouin-zone (BZ) integrations 512 **k** points within the BZ have been used during the self-consistency cycle and 2744 **k** points for the calculation of the optical spectra. Exchange and correlation effects are accounted for by the local-density approximation parametrized by Perdew and Wang.[19] The interband contribution to the dielectric function is computed within the independent quasiparticle approximation. Intraband contributions show no influence on the dielectric function around the photon energy used in the Raman experiments.

Starting from the experimental data of Ref. 20 for the lattice constants and atom positions, all parameters were optimized by minimizing the pressure and atomic forces, respectively. This procedure turned out to be necessary to describe phonon frequencies and Raman spectra in agreement with experimental data.[12,21] A detailed description of the atomic force computation within the LAPW method is given in Ref. 22. Within the frozen-phonon approach a polynomial fit of calculated atomic-force values is carried out, where in all cases only terms in first order turned out to be important. For the A_{1g} mode this was done for the equilibrium position and four different displacements of each participating atom along the tetragonal c axis. For the E_g mode the equilibrium position and four different displacements of the corresponding atoms parallel to the CuO_2 plane were considered. For both kinds of modes, diagonalization of the dynamical matrix yields the phonon frequencies as well as the normal vectors of the vibrations. Due to the large mass difference of the La (Ba) and O atoms, the A_{1g} modes are nearly decoupled, so that the displacements considered are already displacements along the eigenvector. However, in case of the E_g mode stronger coupling occurs, so that five explicit distortions along the eigenvector were calculated in addition, for the determination of the Raman scattering intensities.

Doping was treated by the virtual crystal approximation,[23] i.e., within a single unit cell with averaged (fractional) nuclear and electronic charges according to the amount of doping. This procedure is well justified by the similar electronic configuration of La $(Z=57)$ and Ba $(Z=56)$. Moreover, the La (Ba) states are far from the Fermi level and thus hardly influence the region of valence bands. An explicit test calculation of phonon frequencies showed that the crystal structure for the doped case can be adapted from the undoped one.

B. Raman spectra

The Raman-scattering intensity $\sigma_{jl}(\omega_R)$ of a given mode ζ with frequency ω_ζ and normal coordinate Q_ζ in a certain scattering geometry (jl) is given as a function of the Raman shift ω_R:[12]

$$\sigma_{jl}(\omega_R)=\frac{N_\Omega\Omega(\omega_I-\omega_R)^3\sum_\mu e^{-E_\mu/k_BT}\sum_\nu [\delta\varepsilon_{jl}^{\mu\to\nu}]^2 L(\omega_R,\omega_{\mu\nu},\Gamma)}{(4\pi)^2c^4\sum_\mu e^{-E_\mu/k_BT}}. \tag{3.1}$$

j and l are Cartesian indices which denote the polarization of the ingoing and outgoing light, respectively. $N_\Omega\Omega$ is the coherent volume with Ω being the unit-cell volume, ω_I is the frequency of the incoming light, and T is the temperature. $L(\omega_R,\omega_{\mu\nu},\Gamma)$ accounts for a broadening of the transitions, and the matrix elements $\delta\varepsilon_{jl}^{\mu\to\nu}$ are given by

$$\delta\varepsilon_{jl}^{\mu\to\nu}=\frac{\partial\varepsilon_{jl}^{\omega_I}}{\partial Q_\zeta}\langle\nu|\hat{Q}_\zeta|\mu\rangle, \tag{3.2}$$

where $|\nu\rangle$ and $|\mu\rangle$ are the initial and final vibrational states with energies E_ν and E_μ. For all relevant scattering geometries (jl) we have computed the dielectric function $\varepsilon_{jl}^{\omega_I}$ for five points along each normal coordinate and fitted the Q_ζ dependence of the dielectric function at the frequency of the incoming light.

C. Electric-field gradients

Another parameter of interest is the electric-field gradient (EFG) as a sensitive probe for the distribution of the elec-

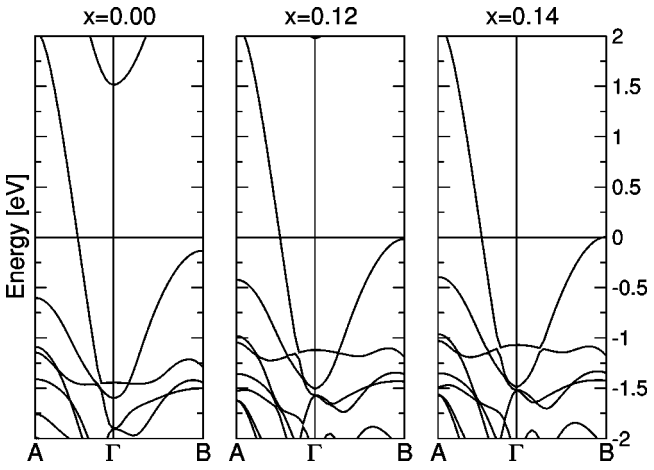

FIG. 1. Band structure of $La_{2-x}Ba_xCuO_4$ for different doping concentrations x. The points A and B correspond to $k_A=(\frac{1}{2},\frac{1}{2},0)$ and $k_B=(0,\frac{1}{2},0)$, respectively, given in Cartesian coordinates and units of $(2\pi/a,2\pi/a,2\pi/c)$. The bands are plotted with respect to the Fermi energy.

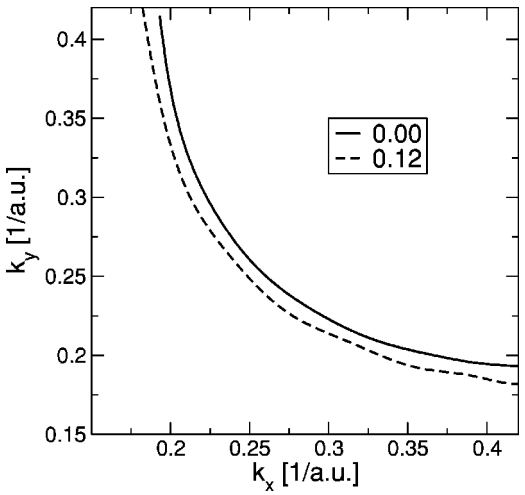

FIG. 2. Intersection of the Fermi surface of $La_{2-x}Ba_xCuO_4$ with the $k_z=0$ plane for the undoped case and for a doping concentrations of $x=0.12$. The Brillouin-zone boundary is reached at $k_{x,y}\approx 0.44$ (a.u.$^{-1}$).

tronic charge in the vicinity of the atomic nuclei. The EFG tensor is defined as the second spatial derivative of the electrostatic potential on the lattice site,

$$V_{jl}=\frac{\partial^2 V}{\partial x_j \partial x_l}. \tag{3.3}$$

When related to its principal axes, only the diagonal elements V_{aa}, V_{bb}, and V_{cc} remain, where the components are ordered according to their magnitude as $|V_{cc}|\geqslant|V_{bb}|\geqslant|V_{aa}|$. A traceless tensor V_{jl} $(V_{aa}+V_{bb}+V_{cc}=0)$ is fully characterized either by its components or by the principal value V_{cc} and an asymmetry parameter η is defined as

$$\eta=\frac{V_{aa}-V_{bb}}{V_{cc}}. \tag{3.4}$$

In the case of tetragonal or higher site symmetry of the atom in question the parameter η is zero.

IV. RESULTS AND DISCUSSION

A. Electronic structure

The band structure of the undoped material has, for example, been discussed in Ref. 24. As obtained by our self-consistent calculations for different Ba concentrations, the doping can be well understood in a rigid-band picture, where the main effect is a shift of the Fermi level from higher to lower energies (hole doping). This finding has been published previously in connection with an anomaly in a zone-edge mode.[16] The band crossing the Fermi level is shown for different doping concentrations in Fig. 1. As one can see there the effect of doping is twofold. First, it causes a partial depopulation of the CuO_2 band. As a consequence, the intersection of this band with the Fermi energy, E_F, is shifted to smaller wave vectors resulting in an increased Fermi-surface (FS) area (Fig. 2). At the same time a Van Hove singularity moves up to the Fermi level, touches it at optimal doping, and crosses E_F slightly in the overdoped case creating a small hole pocket at $k_B=(0,\frac{1}{2},0)$. This latter effect also shows up in the density of states which is plotted in Fig. 3 for different doping concentrations x. At optimal Ba content a peak in the DOS is situated right at the Fermi level. In the large graph only the curves for the undoped $(x=0)$ and the overdoped $(x=0.14)$ cases are depicted. It can be seen that doping causes a general shift to the right. This effect is more pronounced for the unoccupied bands. The inset shows the DOS around the Fermi energy for several doping levels clearly exhibiting a local maximum at E_F for optimal doping.

Since the superconducting mechanism is usually treated within models using a parametrization of the band structure, in particular, of the Cu-O derived bands, we have also calculated the parameters for a tight-binding representation of this band. The change of these parameters with doping is quite small. The Cu-O hopping matrix element t slightly in-

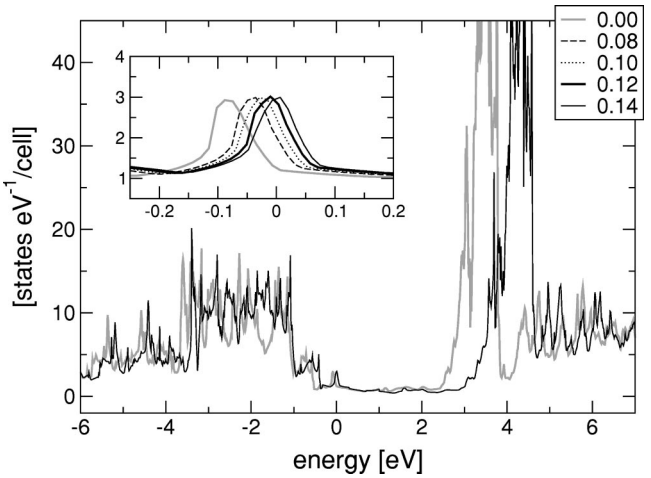

FIG. 3. Total DOS for different doping concentrations x. The inset shows a magnification of the DOS around the Fermi energy.

TABLE I. Selected partial charges of Cu-$d_{x^2-y^2}$ and O1-p_x analyzed within the atomic spheres of Cu and O1, respectively. Δholes indicates the corresponding increase of the number of holes upon doping.

Doping	Cu-$d_{x^2-y^2}$	O1-p_x	Δholes
0.00	1.433	1.094	0.000
0.08	1.415	1.084	0.038
0.10	1.411	1.082	0.046
0.12	1.406	1.079	0.057
0.14	1.403	1.077	0.064

creases from 0.729 eV at $x=0$ to 0.743 eV at $x=0.12$. In contrast, the O-O hopping matrix element t' decreases from 0.598 eV to 0.575 eV, making the ratio t'/t decrease by 6%. In comparison to $YBa_2Cu_3O_7$, t'/t is large and has some consequences for the Raman-scattering intensities as one will see later.

The doping-dependent population of the CuO_2 band also shows up in a redistribution of the charge density which can be analyzed within the atomic spheres exploiting the atomiclike basis set of the LAPW method. The corresponding partial charges of Cu-$d_{x^2-y^2}$ and O1-p_x can be seen in Table I. As expected, the charge of the CuO_2-plane-originated band decreases upon doping. For optimal doping the number of doping-induced holes is around 0.06e which is roughly a factor-of-2.5 smaller than in the case of $HgBa_2CuO_4$.[25] This fact can be related to the much lower T_c of $La_{2-x}Ba_xCuO_4$. It should be noted that the decrease of the Cu-$d_{x^2-y^2}$ and O1-p_x occupation numbers is accompanied by a slight increase of the O1-p_y and O1-p_z charges (0.007e and 0.008e, respectively), which is a measure for the deviation from the pure rigid-band behavior.

The charge redistribution also causes changes in the electric-field gradients. The doping dependence of the EFG's is given in Table II, where the principal component for all atoms in the unit cell and the asymmetry parameter η for O1 are listed. Only the latter atom has a nonzero η value due to its lower site symmetry (mmm). As described in detail for $YBa_2Cu_3O_7$,[26] the oxygen EFG points into the direction of the lowest partial p charge, which is the b direction for O1 and the c direction for O2. Also the La/Ba EFG and the Cu EFG point into the c direction. For copper and the plane oxygen the decrease of the occupation numbers results in a linear increase of the absolute value of the EFG, which is in the range from $x=0$ to $x=0.14$, 25% and 16%, respectively. In particular, the V_{yy} component of O1 increases which could give rise to an enhanced asymmetry parameter η. Due to an increased V_{zz} component, however, η is even slightly decreased. The most pronounced relative change (-28%) is found for the apical oxygen O2, although its magnitude is very small, which is in accordance with NMR measurements for $La_{1.85}Sr_{0.15}CuO_4$.[27] Although the La/Ba position should not be interpreted in detail due to its averaged treatment, the doping dependence of the EFG at this site indicates only a very minor effect when La is replaced by Ba. This finding reproduces the experimental situation, where the corresponding EFG was measured to be 17.6×10^{21} V/m^2 for the undoped[28] as well as for the Sr-doped material $La_{1.85}Sr_{0.15}CuO_4$.[29] An explanation is provided by the ionic behavior of the La (Ba, Sr) site. The theoretical underestimation of the copper EFG in the CuO_2 planes of the high-T_c cuprates has been discussed in Ref. 26 and is also found for this compound.

TABLE II. Electric-field gradient V_{zz} for all atoms in the unit cell in 10^{21} (V/m^2). Note that due to the lower site symmetry (mmm) only the O1 oxygen has a nonzero asymmetry parameter η.

Doping	La/Ba	Cu	O1				O2
x	V_{zz}	V_{zz}	V_{xx}	V_{yy}	V_{zz}	η	V_{zz}
0.00	-18.8	-5.9	-6.1	8.8	-2.8	0.38	-2.4
0.08	-18.5	-6.8	-6.4	9.6	-3.2	0.33	-2.1
0.10	-18.4	-7.0	-6.5	9.8	-3.3	0.32	-2.0
0.12	-18.3	-7.2	-6.6	10.0	-3.5	0.31	-1.9
0.14	-18.2	-7.4	-6.7	10.2	-3.6	0.30	-1.7

TABLE III. Frequencies ω (in cm^{-1}) and eigenvectors of the A_{1g} and E_g modes for different doping concentrations x. The third (sixth) and the fourth (seventh) columns indicate the relative La/Ba and O2 displacements of the corresponding vibration.

A_{1g}		O2 mode			La/Ba mode	
x	ω	La/Ba	O2	ω	La/Ba	O2
0.00	382	0.13	0.99	211	-0.99	0.13
0.08	382	0.12	0.99	210	-0.99	0.12
0.10	382	0.12	0.99	209	-0.99	0.12
0.12	381	0.12	0.99	209	-0.99	0.12
0.14	381	0.12	0.99	208	-0.99	0.12
E_g		O2 mode			La/Ba mode	
x	ω	La/Ba	O2	ω	La/Ba	O2
0.00	205	0.35	-0.94	27	0.94	0.35
0.08	206	0.33	-0.94	42	0.94	0.33
0.10	207	0.32	-0.95	45	0.95	0.32
0.12	207	0.32	-0.95	47	0.95	0.32
0.14	207	0.31	-0.95	51	0.95	0.31

B. Phonons and Raman spectra

The frequencies of the A_{1g} and E_g modes and the corresponding eigenvectors as a function of doping can be found in Table III. It can be seen from the eigenvectors that the contributions of La/Ba and O ions in the A_{1g} modes are almost decoupled, whereas the E_g coupling is a little stronger. This behavior is almost unaffected by doping. While the A_{1g}-mode frequencies hardly change with the Ba content, there is a linear increase in the frequency of the lower E_g mode. For the undoped case, all frequencies are in very good agreement with published theoretical values.[4]

In the case of Sr doping, experimental data for Raman spectra and frequencies can be found in Refs. 5 and 30, and

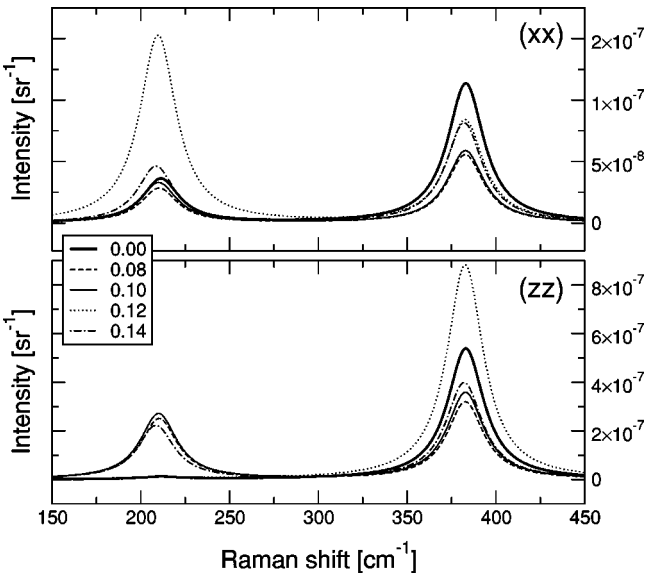

FIG. 4. Low-temperature A_{1g} spectra in (xx) and (zz) polarizations for different doping concentrations x in $La_{2-x}Ba_xCuO_4$. The laser light wavelength was chosen to be 514 nm. According to the Raman tensor in Eq. (2.1), the (xx)- and (yy)-polarized spectra are equal. The broadening Γ was chosen to be 25 K.

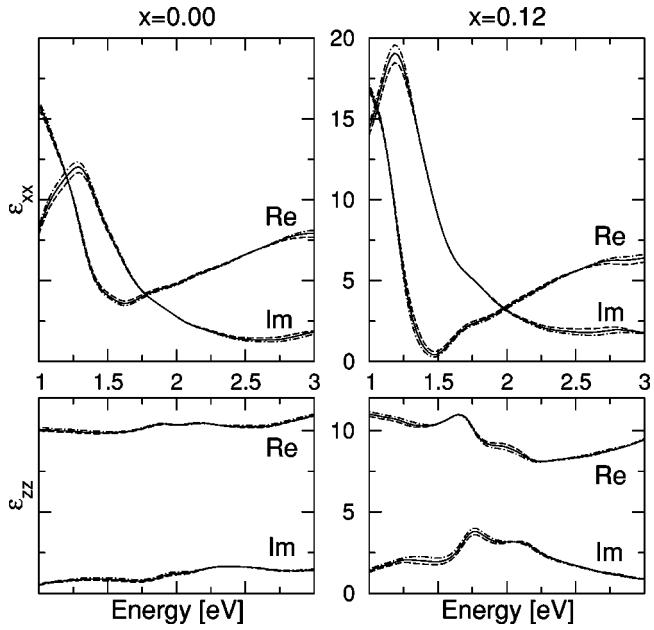

FIG. 5. Real and imaginary parts of the dielectric function ϵ for different displacements of the La/Ba atom in the optimal doped ($x=0.12$) and undoped cases. The solid line corresponds to the equilibrium position and the other lines depict two displacements, namely, one to each side of the equilibrium position.

reference therein. Our calculated Raman spectra for the A_{1g} modes are depicted in Fig. 4. The laser light wavelength was chosen to be 514 nm (2.41 eV) which is often used in Raman-scattering experiments. In the upper panel the (xx) polarization is pictured. The lower panel shows the (zz) polarization, where the intensities are clearly larger than in (xx), which is analogous to $YBa_2Cu_3O_{7-x}$, where the main contribution to the Raman intensity comes from the apical oxygen close to the CuO chains[31] and thus is (zz) polarized. In both scattering geometries the spectra undergo a huge intensity change around the optimal Ba concentration. This is an indication for an increase of electron-phonon coupling with doping. In particular, the phonon-mediated change of the polarizability of the crystal is strongly enhanced. It should be noted that it is not caused by a change of the phonon eigenvectors which stay practically the same. It is, however, related to the creation of the hole pocket[16] in the following way. Since at optimal doping the Van Hove singularity is located right at E_F, the phonon displacement can make it pass through E_F, and thus initial states for possible dipole transitions are gained or lost during the vibration. Hence, the dielectric function can be strongly altered and resonance effects can occur as discussed in Ref. 32. But also the phonon-induced redistribution within the Cu-O band can have a pronounced effect on the Raman intensities. Given the **k**-dependent electron-phonon matrix element $g(\mathbf{k})$ for the states near the Fermi surface, the local deformation of the FS is proportional to $[g(\mathbf{k})-\langle g(\mathbf{k})\rangle]/v_F$,[32,33] with v_F being the Fermi velocity. Integrating over the FS, the change in the polarizability is proportional to the DOS at E_F, $N(E_F)$, times a factor which is a measure for the anisotropy of the electron-phonon coupling and proportional to t'/t.[34] Thus, such a contribution to the polarizability scales with $N(E_F)\ t'/t$. The corresponding Raman intensity would be proportional to the square of this expression. Since, as mentioned before, t'/t is rather large in this compound, the corresponding effect can be significant.

Having a closer look at the dielectric functions and their changes upon displacements and doping (see Figs. 5 and 6)

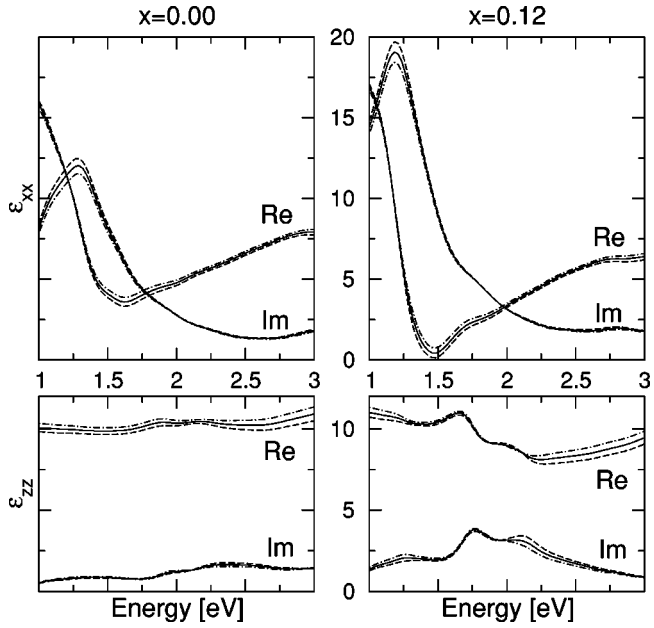

FIG. 6. Real and imaginary parts of the dielectric function ϵ for different displacements of the O2 atom in the optimal doped ($x=0.12$) and undoped cases. The solid line corresponds to the equilibrium position and the other lines depict two displacements, namely, one to each side of the equilibrium position.

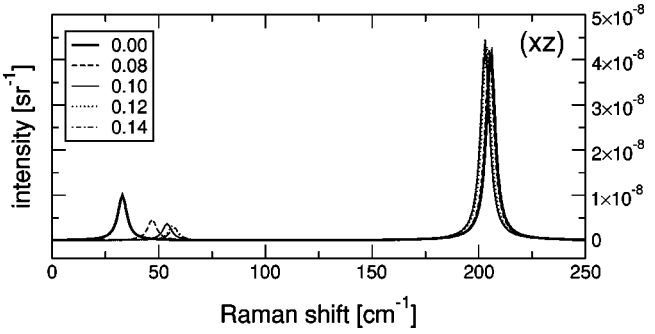

FIG. 7. Low-temperature E_g spectra in (xz) polarization for different doping concentrations x in $La_{2-x}Ba_xCuO_4$. The laser light wavelength was chosen to be 514 nm and the broadening Γ, 5 K.

one realizes that the phonon-induced changes strongly depend on the photon energy. We therefore predict that the Raman intensities for both modes should be much higher in the infrared region (between 1 and 1.7 eV) and also between 2.5 and 3 eV. Depending on the mode and the energy range, quite pronounced doping effects can be expected.

The Raman spectra for the E_g modes are given in Fig. 7 for the same wavelength of incident light. Due to the Raman tensor for this mode given in Eq. (2.2), only the (xz) [and the equivalent (yz)] spectrum is nonvanishing. The intensity of the whole spectrum is smaller by one order of magnitude compared to the A_{1g} scattering. Upon doping the linear shift of the lower frequency can be observed, accompanied by an intensity decrease. For the 205 cm^{-1} mode no change in intensity is found.

The measured A_{1g} O2 frequencies differ in the range from 380 to 432 cm^{-1}, while the La mode was found at 226 or 231 cm^{-1}, respectively. Therefore both calculated frequencies are in reasonable agreement with experiment. For the E_g mode the experimental discrepancy is even bigger: values of 180, 231, and 367 cm^{-1} have been assigned to the E_g O2 mode.[30] The only available experimental value assigned to the E_g La vibration is 149 cm^{-1}. However, this measurement does not seem to correspond to the E_g La mode since theory predicts a value of 27 cm^{-1} in agreement with previous findings.[4] When doped with Sr the experimental A_{1g} O2 frequency decreases slightly,[30] which is parallel to our findings for the Ba doping.

The comparison of experimental A_{1g} Raman spectra for the case of Sr doping,[5] with the calculated spectra for Ba doping, exhibits several similarities. In (zz) polarization the measured A_{1g} O2 intensity decreases upon replacement of La by Sr, is about the smallest for $x \sim 0.09$, and increases again for $x > 0.09$. The same behavior is found theoretically for Ba doping. However, the large increase for optimal Ba doping is not present in the experimental situation. Also the change of the A_{1g} La intensity as a function of doping, i.e., starting from an almost vanishing value for small doping concentrations followed by a huge increase, is parallel to our findings. Furthermore, the measured intensity ratio of the A_{1g} O2 and A_{1g} La modes is comparable to the calculated spectra. The comparison of experimental and theoretical results for the (xx) scattering geometry is somewhat more complicated. These intensities are smaller by one order of magnitude and therefore more noise is present in the measured data. However, experiment and theory give a minimum intensity of the A_{1g} O2 mode for $x \sim 0.1$. Again, the large increase for optimal Ba doping is not present in the experimental situation. Also, in this polarization the measured intensity ratio of the O2 and La modes is comparable to the calculated spectra.

V. CONCLUSIONS

In summary, we have carried out calculations on the electronic structure and Raman spectra of $La_{2-x}Ba_xCuO_4$. It turned out that this material shows pronounced effects as a function of doping. In particular, we find a charge redistribution within the CuO_2 planes leading to an increase of holes in this plane. This can be probed by electric-field gradients which are sensitive to the distribution of the electronic charge in the vicinity of the atomic nuclei. With doping, a peak in the DOS moves up close to the Fermi level and reaches a maximum at optimal doping. Moreover, the change in the Raman intensities points to a strong increase of electron-phonon coupling near x_{opt}. The similarities of all our findings for the Ba-doped compound with experimental results for the Sr-doped compound underline the same physical effects introduced by the two different dopant atoms. Our findings suggest that electron-phonon coupling may play an important role for this relatively low-T_c cuprate, and thus supports the claims of Refs. 2 and 3.

ACKNOWLEDGMENTS

We are thankful for fruitful discussions with E. Ya. Sherman. Part of this work was supported by the Austrian Science Fund Project Nos. P14004-TPH and P13430-PHY.

[1] J. G. Bednorz and K. A. Müller, Z. Phys. B: Condens. Matter **64**, 189 (1986).

[2] Z.-X. Shen, A. Lanzara, S. Ishihara, and N. Nagaosa, Philos. Mag. B **82**, 1349 (2002).

[3] A. Lanzara, P. V. Bogdanov, X. J. Zhou, S. A. Kellar, D. L. Feng, E. D. Lu, T. Yoshida, H. Eisaki, A. Fujimori, K. Kishio, J. -I. Shimoyama, T. Noda, S. Uchida, Z. Hussain, and Z.-X. Shen, Nature (London) **412**, 510 (2001).

[4] C. Z. Wang, R. Yu, and H. Krakauer, Phys. Rev. B **59**, 9278 (1999).

[5] D. Lampakis, D. Palles, E. Liarokapis, C. Panagopoulos, J. R. Cooper, H. Ehrenberg, and T. Hartmann, Phys. Rev. B **62**, 8811 (2000).

[6] G. Burns, G. V. Chandrashekhar, F. H. Dacol, and M. W. Shafer, Solid State Commun. **68**, 67 (1988).

[7] M. Copic, D. Mihailovic, M. Zgonik, M. Prester, K. Biljakovic,

B. Orel, and N. Brnicevic, Solid State Commun. **64**, 297 (1987).
[8] T. Brun, M. Grimsditch, K. E. Gray, R. Bhadra, V. Maroni, and C. K. Loong, Phys. Rev. B **35**, 8837 (1987).
[9] S. Sugai, Phys. Rev. B **39**, 4306 (1989).
[10] S. Sugai, S. Shamoto, M. Sato, T. Ido, H. Takagi, and S. Uchida, Solid State Commun. **76**, 371 (1990).
[11] K. Schwarz, Solid State Commun. **64**, 421 (1987).
[12] C. Ambrosch-Draxl, H. Auer, R. Kouba, E. Ya. Sherman, P. Knoll, and M. Mayer, Phys. Rev. B **65**, 064501 (2002).
[13] P. Puschnig, C. Ambrosch-Draxl, R. W. Henn, and A. Simon, Phys. Rev. B **64**, 024519 (2001).
[14] R. J. McQueeney, Y. Petrov, T. Egami, M. Yethiraj, G. Shirane, and Y. Endoh, Phys. Rev. Lett. **82**, 628 (1999).
[15] L. Pintschovius and M. Braden, J. Low Temp. Phys. **117**, 437 (1999).
[16] T. Thonhauser and C. Ambrosch-Draxl, Physica C **341-348**, 281 (2000).
[17] R. M. Fleming, B. Batlogg, R. J. Cava, and E. A. Rietman, Phys. Rev. B **35**, 7191 (1987).
[18] P. Blaha, K. Schwarz, G. Madsen, D. Kvasnicka, and J. Luitz, WIEN2k, *An Augmented Plane Wave+Local Orbitals Program for Calculating Crystal Properties* (Karlheinz Schwarz, Techn. Universität Wien, Austria, 2001).
[19] J. P. Perdew and Y. Wang, Phys. Rev. B **45**, 13 244 (1992).
[20] J. D. Jorgensen, H. B. Schüttler, D. G. Hinks, D. W. Capone II, K. Zhang, M. B. Brodsky, and D. J. Scalapino, Phys. Rev. Lett. **58**, 1024 (1987).
[21] R. Kouba, C. Ambrosch-Draxl, and B. Zangger, Phys. Rev. B **60**, 9321 (1999).
[22] R. Kouba and C. Ambrosch-Draxl, Phys. Rev. B **56**, 14 766 (1997).
[23] J. S. Faulkner, in *Progress in Materials Science*, edited by J. W. Christian, P. Haasen, and T. B. Massalski (Pergamon, London, 1982), Vol. 27.
[24] W. E. Pickett, Rev. Mod. Phys. **61**, 433 (1989).
[25] C. Ambrosch-Draxl, P. Süle, H. Auer, and E. Y. Sherman, Phys. Rev. B **67**, 100505 (2003).
[26] K. Schwarz, C. Ambrosch-Draxl, and P. Blaha, Phys. Rev. B **42**, 2051 (1990).
[27] E. Oldfield, C. Coretsopoulos, S. Yang, L. Reven, H. C. Lee, J. Shore, O. H. Han, E. Ramli, and D. Hinks, Phys. Rev. B **40**, 6832 (1989).
[28] H. Nishihara, H. Yasuoka, T. Shimizu, T. Tsuda, T. Imai, S. Sasaki, S. Kanbe, K. Kishio, K. Kitazawa, and K. Fueki, J. Phys. Soc. Jpn. **56**, 4559 (1987).
[29] H. Lütgemeier and M. W. Pieper, Solid State Commun. **64**, 267 (1987).
[30] I. Ohana, M. S. Dresselhaus, Y. C. Liu, P. J. Picone, D. R. Gabbe, H. P. Jenssen, and G. Dresselhaus, Phys. Rev. B **39**, 2293 (1989).
[31] E. I. Rashba and E. Ya. Sherman, Pis'ma Zh. Éksp. Teor. Fiz. **47**, 404 (1988) [JETP Lett. **47**, 482 (1988)].
[32] E. Ya. Sherman and C. Ambrosch-Draxl, Eur. Phys. J. B **16**, 251 (2000).
[33] E. Ya. Sherman and C. Ambrosch-Draxl, Phys. Rev. B **62**, 9713 (2000).
[34] E. Ya. Sherman and O. V. Misochko, Phys. Rev. B **63**, 104520 (2001).